Received August 5, 2018, accepted September 13, 2018, date of publication September 19, 2018, date of current version October 17, 2018.

Digital Object Identifier 10.1109/ACCESS.2018.2871059

LTE/Wi-Fi/mmWave RAN-Level Interworking Using 2C/U Plane Splitting for Future 5G Networks

AHMED S. MUBARAK[1,2], (Student Member, IEEE), HAMADA ESMAIEL[1], (Member, IEEE), AND EHAB MAHMOUD MOHAMED[1,3], (Member, IEEE)

[1]Electrical Engineering Department, Faculty of Engineering, Aswan University, Aswan 81542, Egypt.
[2]Electrical Engineering Department, Faculty of Engineering, Sohag University, Sohag 82524, Egypt.
[3]Electrical Engineering Department, College of Engineering, Prince Sattam Bin Abdulaziz University, Wadi Addwasir 11991, Saudi Arabia.

Corresponding author: Ehab Mahmoud Mohamed (ehab_mahmoud@aswu.edu.eg)

This work was supported by the National Telecom Regulatory Authority, Egypt, through the Project "LTE/Wi-Fi/WiGig Internetworking for Future 5G Cellular Networks."

ABSTRACT Integration of the promising millimeter wave (mmWave) technology into the legacy cellular network is one of the main challenges toward a unified 5G cellular network. However, directly controlling the access of mmWave small cells (SCs) via the LTE eNB using the conventional LTE/WLANs interworking seems to be an inefficient solution. This is due to the short transmission range of the mmWave signal accompanied with the inevitable use of directional communications in these bands. In this paper, a novel radio access network-level hierarchical multi-band heterogeneous network (HetNet) is proposed to efficiently overlay mmWave SCs over LTE. In this architecture, the Wi-Fi medium coverage band is used as an intermediate level between the large coverage LTE band and the small coverage mmWave band. The Wi-Fi band via the proposed concept of Wi-Fi/mmWave sub-clouds enables precise control to the access over the mmWave band. Whereas, the LTE eNB only controls the access over the distributed Wi-Fi/mmWave sub-clouds. Accordingly, a novel concept of two-level control and user data (2C/U) planes splitting is introduced in this paper. In this 2C/U plane splitting, the LTE eNB controls the network access over the distributed sub-clouds using the first level of control (C1-plane). The second level of control (C2-plane), provided by the Wi-Fi band, controls the access over the distributed mmWave SCs inside the sub-clouds. Thanks to this distributed control, the mmWave band can be efficiently utilized and the complexity of the mmWave initial access can be highly reduced. Moreover, the associated signaling/processing load on both LTE eNB and core network can be highly relaxed. Analytical and numerical analysis assure the performance superiority of the proposed LTE/Wi-Fi/mmWave HetNet over the conventional LTE/mmWave HetNet.

INDEX TERMS 5G RAN architecture, tight coupling, LTE, Wi-Fi/mmWave sub-cloud, 2C/U splitting.

I. INTRODUCTION

Fifth generation (5G) mobile cellular networks have been envisioned to face the bottleneck of the current cellular networks in supporting the future high wireless data rates [1]–[3]. It is well-recognized that, due to their complementary and attractive features, the cellular networks [4] and wireless local area networks (WLANs) [5] can be integrated into a multi radio access technologies (multi-RATs) heterogeneous networks (HetNets) [6]–[8] enabling high data rate services. In the recent years, the integration between the long term evolution (LTE)/long term evolution-advanced (LTE-A) [4] and WLAN has drawn considerable research attention. To this end, many interworking solutions have been developed by different standard organizations to consider the cellular network/ WLAN integration challenges [9]–[12]. Specifically, the 3rd generation partnership project (3GPP) had been working on standardization for this LTE/WLAN integration and various interworking architectures have been introduced. In these architectures, the LTE eNB is overlaid with WLAN out-of-band small cells (SCs) to enable user traffic offloading and to increase the quality of service (QoS) and the overall system capacity. Generally, according to the interdependence between the mobile network and WLAN, the interworking architectures are classified into two groups,

loosely and tightly-coupled architectures [13], [14]. In the loosely-coupled architecture, the WLAN is connected to 3GPP network using an IP network, e.g., Internet, hence the WLAN performance usually is not under the control of the 3GPP operator. However, in the tightly-coupled approach, the 3GPP network infrastructures and protocols can be reused, since WLAN can be connected to 3GPP core network (CN) or integrated into a specific 3GPP radio access network (RAN) protocol stack layer. In that context, CN-level and RAN-level tightly-coupled LTE/WLAN integration solutions have been investigated in different 3GPP releases [15], [16]. In these architectures, the WLAN becomes under the full control of the 3GPP operator and the overall system performance can be increased by jointly control and optimize the network resources in the LTE eNB as an anchor point. Moreover, control/user (C/U) plane splitting and dual connectivity (DC) concepts have been proposed to reduce the CN frequent handover (HO) signaling [17], [18]. The C/U plane splitting and DC allow the user equipment (UE) to connect with more than one SC simultaneously, since the C-plane is provided by the large footprint LTE eNB while the U-plane is opportunistically provided by the SCs.

Although LTE/WLAN integration can relatively improve the total system capacity, it could not meet the huge 5G data rate demands due to the limited bandwidth in the two-legacy integrated access networks, e.g., LTE and Wi-Fi. Recently, the huge amount of bandwidth available in the millimeter wave (mmWave) band, 30 $\sim$ 300 GHz, [19]–[22] has a general consensus in both academia and industry as a key player for constituting multi-gigabit 5G wireless networks. In this context, inspired by the different outdoor applications of WLANs [23], integrating the mmWave enabled WLAN with the legacy LTE networks can fulfill the requirements and challenges of future 5G networks. However, operating at such high frequencies makes mmWave suffering from higher propagation and penetration losses and blockage due to human and obstacles. This in turns limits the mmWave transmission range to be a few meters around the mmWave SC and prevents to efficiently unleash its potentials [24]. To mitigate these issues, directional transmission using array antenna is considered for providing longer transmission ranges and enabling mmWave communications [22], [25]. Moreover, network densification as a key mechanism for future 5G systems [26]–[28] can significantly robust the mmWave communications. This can be done by increasing the probability that a UE can be serviced from different mmWave SCs. However, many challenges, such as energy consumption and backhauling, need to be tackled towards the efficient realization of the ultra-dense networks [28]. From the standardization point of view, the Wireless Gigabit Alliance (WiGig) standard, also known as IEEE 802.11ad standard [29], was developed to support multi-gigabit WLAN in the 60 GHz unlicensed band. According to the WiGig standard, an exhaustive search medium access control (MAC) based beamforming training (BT) protocol is proposed for enabling mmWave link establishment.

Aforementioned mmWave limitations and special features make its integration into the LTE cellular network more challenging than the conventional LTE/WLAN integration. Since, many critical issues such as mmWave SC discovery and association, mmWave SCs coordination, coordinated BT among mmWave SCs, mmWave SCs seamless handover (HO), etc. [30], should be efficiently addressed while performing integration with the LTE eNB. Moreover, the deployment of the limited-coverage mmWave SCs to fully cover the large LTE eNB footprint will highly increase the complexity and power consumption rates. This is because, LTE eNB needs to manage the mmWave challenging issues over thousands of deployed mmWave SCs simultaneously. The consequences will be more worse in the case of mobility scenario, since a moving UE needs to change its serving SC more frequently. Also, inside the serving mmWave SC, re-beamforming using an exhaustive search BT process is required to maintain the communication link when the UE moves away from the serving beam coverage. Such frequent beam and SC HOs cause heavy mobility signaling load on both LTE eNB and CN. Due to the newly arising mmWave challenges, direct usage of the currently standardized and proposed LTE/WLAN integration architectures, without appropriate modifications, wastes the huge resources provided by the mmWave band.

In this perspective, this paper addresses the challenge of LTE/mmWave integration and proposes a novel interworking solution based on the interplay between different RATs in a hierarchical HetNet architecture. In the proposed HetNet, without loss of generality, Wi-Fi is used as an intermediate band between LTE and mmWave bands to precisely manage the mmWave access via the proposed concept of Wi-Fi/mmWave sub-clouds. Towards that, a novel 2C/U plane splitting mechanism is also proposed to orchestrate the interoperation between the different RATs. In which, the two-level C-plane is distributed between the LTE and Wi-Fi bands, while the U-plane is mainly attached to the highest data rate mmWave band. The first control plane, C1, is attached to the LTE eNB and it controls the access between the LTE eNB and the deployed Wi-Fi/mmWave sub-clouds and among the sub-clouds. The second control plane, C2, is attached to the Wi-Fi band, and it controls the access among Wi-Fi/mmWave SCs inside each sub-cloud. LTE-based localization service is used to provide relatively accurate UE location information in the sub-cloud domain. Hence, LTE eNB can efficiently manage the sub-clouds discovery, synchronization and association. Inside, each sub-cloud, the mobility associated signaling can be maintained in a local management domain by introducing what so-called sub-cloud local controller (SLC). Assisted by an accurate Wi-Fi-based localization service [31], the SLC can precisely manage and control the access over the mmWave SCs in its associated sub-cloud using Wi-Fi signaling provided by the C2 plane. Utilizing the unlicensed Wi-Fi band is inspired by its precise control over the mmWave access at lower implementation cost. This is because, IEEE 802.11ad has a backward compatibility with the IEEE 802.11 Wi-Fi standard and a multi-band

(2.4, 5 and 60 GHz) access point (AP) has already been introduced by IEEE 802.11ad [26]. Moreover, it has interference immunity with the LTE band unlike using other types of LTE medium coverage SCs like picocells and femtocells. Hence, a significant network capacity gain can be achieved using low-cost integration architectures. Due to the proposed hierarchal control, a significant signaling load reduction on the cellular network can be attained, since the heavy mmWave mobility signaling becomes transparent with respect to LTE eNB and CN. Also, the complexity of the mmWave initial access can be extremely reduced due to the accurate Wi-Fi positioning.

The work presented in this paper is related to our conference paper presented in [32], by which comprehensive study and evaluation of the proposed HetNet will be given. Compared to the work presented in [32], in this paper, we will develop the detailed mathematical frameworks for the crucial parameters bounding the performance of the proposed HeNet, such as the miss detection and the false detection probabilities. In addition, the effect of path blocking as a key feature of the mmWave systems will be considered. Furthermore, extensive simulations are conducted to evaluate the performance of the proposed HetNet, since the simulations are extended to include new evaluation metrics such as mmWave initial access complexity. Also, different simulation scenarios with different UE velocities will be presented to evaluate the eNB/CN signaling load in both the proposed multiband HetNet and the conventional one.

Hence, the key contributions of this paper can be summarized as:

- A novel LTE/Wi-Fi/mmWave HetNet architecture is proposed.
- A novel 2C/U plane splitting scheme is proposed to efficiently organize the operation inside the proposed HetNet.
- The detailed protocol stack of the proposed HetNet using an integration in the packet data convergence protocol (PDCP) layer is introduced.
- Mathematical frameworks for the key parameters of the proposed HetNet such as, miss detection and false detection probabilities are driven.
- Extensive simulations to analyze and evaluate the different aspects of the proposed HetNet and compare it with the conventional one are conducted.

The rest of this paper is organized as follows, Section II explores the related works. Section III gives the proposed system model. Section IV gives the proposed 2C/U plane splitting and the proposed protocol stacks. Section V and VI give the mathematical and simulation analysis followed by the conclusion in Section VII.

II. RELATED WORKS

The attractive and complementary characteristics of the cellular networks and WLANs have been drawing considerable research and standards organizations attention and many interworking solutions have been recently proposed in literature. The media independent handover (MIH) framework and the access network query protocol (ANQP) [9], [10] have been developed by IEEE to provide vertical handovers between different RANs, and to support connecting to WLANs, respectively. WiMAX also proposed solutions for interworking with other RANs [12]. In the recent years, 3GPP has specified the high-level interworking requirements and architectures for 3GPP/WLAN integration [33], and it has proposed many interworking solutions, extended from loosely-coupled to tightly-coupled architectures throughout different Releases. In Release 6, the interworking between the 3G (UMTS) and WLAN was investigated [33], and various interworking scenarios have been introduced. In Release 8, the access network discovery and selection function (ANDSF) [11] is introduced to enable UE to discover non-3GPP access networks in non-roaming scenarios, and then it was enhanced in Release 9 [34] to include the roaming scenarios. All the above-mentioned interworking solutions till 3GPP Release 11 are classified as loosely-coupled, which are used to preserve the cellular network resources by providing best-effort traffic to WLANs. The most dominant drawback of this architectural model is the longer handover latencies compared to the tightly-coupled architectural model. In 3GPP Release 12 [16], 3GPP started to identify tightly-coupled interworking solutions using CN-level interworking solutions for LTE/Wi-Fi. In which, the Wi-Fi AP accesses the 3GPP authentication authorization accounting (AAA) server and packet data network gateway (PDN GW) in the 3GPP CN using STa, S2a and S2c interfaces. Recently, 3GPP Release 13 [15] has introduced LTE/WLAN aggregation (LWA) to aggregate the two access networks at the PDCP layer. In these RAN-level architectures, the C/U plane splitting mechanism is introduced to reduce the inter-cell HOs.

Targeting the integration of the promising mmWave band, Semiari *et al.* [35], [36] have proposed two network architectures to directly integrate the sub-6 GHz and mmWave RATs either through the PDCP layer or the MAC layer. Moreover, they proposed resource and mobility management in addition to user application scheduling in the suggested integrated architectures. Also, Li *et al.* [37] and Peng *et al.* [38] have proposed tightly coupled LTE/mmWave integration solutions. In these architectures [34]–[37], the mmWave SCs are directly connected with the LTE eNB via X2 interfaces in a centralized control manner or integrated through the MAC layer in a dual-mode approach. However, due to its unique features, directly integrating mmWave SCs with LTE eNB using the above-mentioned interworking solutions, either loosely coupling or tightly coupling, seem to be inefficient. This is due to the huge signaling control required to manage the access over thousands of mmWave SCs deployed in the LTE eNB area. Also, the accuracy of the LTE-based UE localization, used for taking mmWave HO decisions, is in order of tens of meters, causing numerous false mmWave HO decisions. In addition, LTE-based localization cannot be

used for accomplishing the detailed mmWave radio resource management (RRM) such as finding the best communicating beam IDs, mmWave SCs coordination, coordinated BT among mmWave SCs, mmWave SCs concurrent transmissions, interference management among mmWave SCs, etc. [30].

III. PROPOSED LTE/Wi-Fi/mmWave HetNet

In the followings, we will explain in more details the proposed 5G cellular network based on tightly coupling LTE/Wi-Fi/mmWave bands in a novel hierarchal structure empowered by a newly proposed concept of 2C/U plane splitting.

A. OVERALL HetNet ARCHITECTURE

Fig.1 shows the proposed multi-band HetNet architecture consisting of the wider/continuous coverage LTE eNB overlaid by a few number of Wi-Fi/mmWave sub-clouds. Each sub-cloud represents a cluster including many dual band Wi-Fi/mmWave SCs connected to a SLC. According to the 3GPP standard, the LTE eNB is connected to the mobility management entity (MME) by means of the S1-C interface, and to the serving gateway (SGW) by means of the S1-U interface [39]. As indicated in Fig. 1, the proposed multi-RAT architecture is based on a multi-level anchoring mechanism making it highly compatible with the future concept of wireless caching [40]. In the first level, the LTE eNB is used as the main data anchor point for the UE and the SLCs (sub-clouds), since the U-plane can be provided directly over the lower data rate of LTE radio or opportunistically through WLAN unlicensed radio bands based on WLAN availability. In the second level, the SLC is used as a local data anchor point for the SCs that deployed within the associated sub-cloud, and it decides traffic steering between either Wi-Fi or mmWave band based on the availability. Thus, the data path from the eNB to the SLC remains the same as long as the UE mobility is within the same sub-cloud. On the UE side, multi-band LWA can be performed using the different LTE, Wi-Fi and mmWave modules. To safe the UE energy, the Wi-Fi and mmWave modules remain in the turn-off state and triggered to the turn-on state only when the Wi-Fi and mmWave links are available, respectively.

In the proposed multi-band HetNet, instead of the conventional CN-based and RAN-based interworking architectures using C/U plane splitting [17], a two-stage of internetworking and control is introduced. In the inter sub-cloud stage, when the user is only covered by LTE eNB, its context information, e.g., current position, traffic demand, etc., and the signaling information related to mobility management, radio resource allocations, etc., are conveyed via a C1-plane attached to the LTE eNB. Whereas, on the intra sub-cloud stage, when the UE is located inside a Wi-Fi/mmWave sub-cloud, the LTE may inform the UE to offload its traffic through the selected sub-cloud. Then, all signaling information required for managing user traffic transmissions inside the sub-cloud are conveyed by C2-plane attached to the Wi-Fi band, where

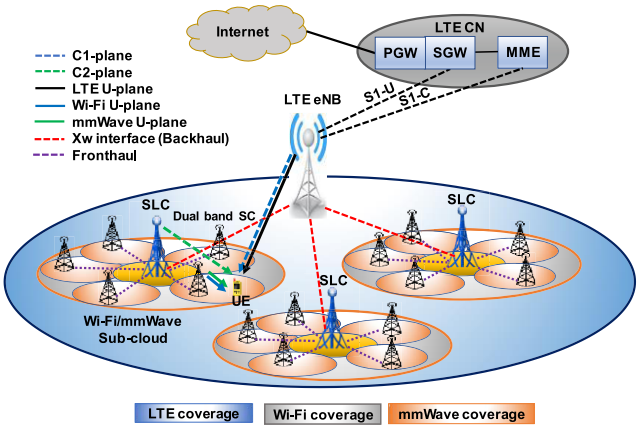

FIGURE 1. Proposed LTE/Wi-Fi/mmWave HetNet architecture.

the SLC carries out most RRM over the sub-cloud without LTE eNB involvement.

B. SUB-CLOUD ARCHITECTURE

As shown in Fig. 1, SLCs are tightly connected to the LTE eNB via high speed backhaul links. To work side by side with the 3GPP standard release 13, Xw interface is employed in the backhaul [13], [15], which represents a logical link that does not require a direct physical interface. Instead, it is based on a tunneling concept, where each connected node can be reached through routing in the IP network. Dual band Wi-Fi/mmWave SCs are connected to a SLC through high speed front-haul links in a cluster fashion. SLC can be implemented as an independent node or employed in one SC in the sub-cloud by providing some controlling functionalities. Inside the sub-cloud, SCs share the same service set identifier (SSID) as a one extended service set (ESS) corresponding to the ''WLAN mobility set''. Also, efficient dual MAC protocols, such as that proposed in [41], can be implemented to organize its internal operation.

The main SLC functions can be summarized as follows:

1) Receiving/forwarding data packets from/to LTE eNB/sub-cloud SCs.
2) Receiving/forwarding only necessary signaling information from/to LTE eNB.
3) Providing a local mobility management by tracking UE position relative to the surrounding SCs.
4) Providing the required signaling for setting up mmWave link via the already established Wi-Fi link.
5) Providing the required signaling for horizontal HO between mmWave SCs and vertical HO between Wi-Fi and mmWave bands.
6) Interference mitigation between operating SCs either in Wi-Fi band by prober radio resource allocation and in mmWave band by eliminating collisions resulting from beams overlap.

By the above-mentioned functionalities, SLC separates the problems of mmWave access and mmWave RRM from LTE eNB. Thus, the mmWave initial access and HOs between

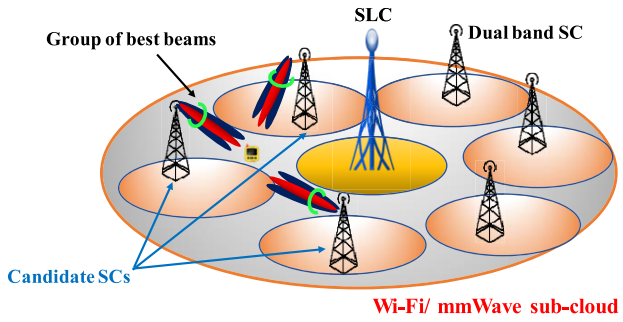

FIGURE 2. Location assisted mmWave initial access.

SCs inside the sub-cloud become transparent to 3GPP network. Accordingly, the signaling/processing load on both LTE eNB and CN will be extremely relaxed. Besides, it reduces the number of frequent HO decisions and latency in data transmissions. This comes due to the use of the more accurate Wi-Fi-based localization and the lower latency front-haul links compared to using LTE-based localization and directly connecting mmWave SCs with LTE eNB via X2 interfaces as proposed in [38].

For mmWave initial access inside the sub-cloud of the proposed HetNet, the scheme in [31] is utilized. In this scheme, as shown in Fig. 2, the SLC selects a group of candidates mmWave SCs expected to cover the UE at its estimated location based on their potential received power strengths. Then, for each candidate mmWave SC, the SLC geometrically localizes a group of best beam IDs to perform BT with the UE based on its estimated location. To overcome localization error, the SLC not only selects the estimated line-of-sight (LOS) beam, but also the first tier of beams around it.

C. LINK PROPAGATION MODELS

In this subsection, the propagation link models of the different LTE, Wi-Fi and mmWave bands are presented.

1) LTE LINK MODEL

The 3GPP urban macro channel model [42] is utilized to represent the macro eNB link. The received power at a UE located at a distance d from the eNB in dBm, $\mathcal{P}_r^{LTE}$, is determined as follows:

$$\mathcal{P}_r^{LTE}\,[\text{dBm}] = \mathcal{P}_t^{LTE}\,[\text{dBm}] - PL_d^{LTE}\,[\text{dB}]\,, \tag{1}$$

where, $\mathcal{P}_t^{LTE}$ is the TX power of the eNB in dBm. PL_d^{LTE} represents the distance-dependent path loss experienced by a UE at distance d from the eNB, which can be expressed as:

$$PL_d^{LTE}\,[\,dB] = 128.1 + 37.6log_{10}\left(\frac{d}{d_0^L}\right) + \mathcal{X}_q^L, \tag{2}$$

where d_0^L denotes the reference distance from the eNB, which is equal to 0.1 km. $\mathcal{X}_q^L$ represents the log-norm shadowing term of the LTE band with zero mean and a standard deviation, σ_{LTE}, of 8 dB.

2) Wi-Fi LINK MODEL

The outdoor propagation model introduced in [43] is used for Wi-Fi transmission. The received power in dBm at a UE located at a distance d from a Wi-Fi SC, $\mathcal{P}_r^W$, is determined as follows:

$$\mathcal{P}_r^W\,[\text{dBm}] = \mathcal{P}_t^W\,[\text{dBm}] - PL_d^W\,[\text{dB}]\,, \tag{3}$$

where, $\mathcal{P}_t^W$ is the TX power in dBm of the Wi-Fi SC. PL_d^W represents the path loss in the Wi-Fi signal at a distance d from a Wi-Fi SC, which can be expressed as:

$$PL_d^W\,[\,dB] = 47.2 + 23.2log_{10}\left(\frac{d}{d_0^W}\right) + \mathcal{X}_q^W, \tag{4}$$

where d_0^W denotes to the reference distance from the Wi-Fi SC, which is equal to 5 m. $\mathcal{X}_q^W$ is the log-norm shadowing term of the Wi-Fi band with zero mean and a standard deviation, σ_W, of 7 dB.

3) mmWave LINK MODEL

The mmWave outdoor link model defined in [44], is utilized in this paper. The received power in dBm at a UE located at a distance d from a mmWave SC, $\mathcal{P}_r^m$, is determined as follows:

$$\mathcal{P}_r^m\,[\text{dBm}] = \mathcal{P}_t^m\,[\text{dBm}] + G_{\text{dB}}\,(\Phi, \Theta)\,[\text{dB}] - PL_d^m\,[\text{dB}]\,, \tag{5}$$

where, $\mathcal{P}_t^m$ is the TX power in dBm of the mmWave SC. PL_d^m represents the distance-dependent path loss experienced by a UE at a distance d from a mmWave SC, which can be expressed as:

$$PL_d^m[\text{dB}] = 82.02 + 10n_m log_{10}\left(\frac{d}{d_0^m}\right) + \mathcal{X}_q^m, \tag{6}$$

where d_0^m denotes the reference distance from a mmWave SC, which is equal to 5 m. $\mathcal{X}_q^m$ represents the log-norm shadowing in the mmWave band in dB with zero mean and a standard deviation, σ_m, of 10.3 dB and 14.6 dB for LOS and non-LOS (NLOS) cases, respectively. n_m is the mmWave exponent path loss, with a value of 3.88 for LOS and 2.2 for NLOS.

$G_{\text{dB}}\,(\Phi, \Theta)$ in (5) represents the antenna gain in dB in a certain direction specified by the azimuth and elevation angles Φ and Θ, respectively, which can be expressed as [45]:

$$G_{dB}\,(\Phi, \Theta) = G_{m\text{dB}} - 12\left(\frac{\Phi - \Phi_0}{\Phi_{-3dB}}\right)^2 - 12\left(\frac{\Theta - \Theta_0}{\Theta_{-3dB}}\right)^2, \tag{7}$$

$$G_{m\text{dB}} = \left(\frac{16\Pi}{6.76\Phi_{-3dB}\Theta_{-3dB}}\right), \tag{8}$$

where $G_{m\text{dB}}$ represents the maximum beam gain in dB. Φ_{-3dB} and Θ_{-3dB} are the half power beam width in the azimuth and elevation directions, respectively, and Φ_0 and Θ_0 represent the azimuth and tilt angles of the beam center.

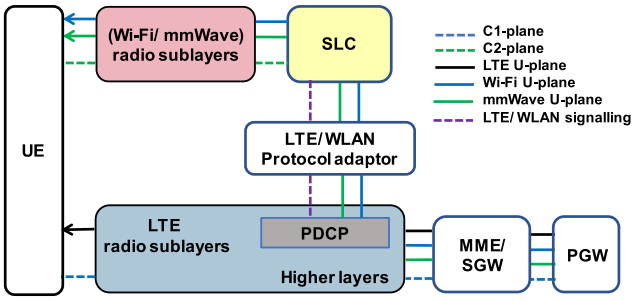

FIGURE 3. Schematic diagram of the proposed LTE/Wi-Fi/mmWave interworking.

IV. PROPOSED 2C/U PLANE SPLITTING AND PROPOSED PROTOCOL STACKS

This section introduces the details of the proposed management protocol and the protocol stacks of the proposed LTE/Wi-Fi/mmWave HetNet. Generally, in building LTE/WLAN interworking architecture, it is necessary to follow the general 3GPP recommendations [15] such as: 1) avoiding any modification/interface in CN, 2) minimizing the impact on IEEE specifications, 3) improving WLAN network control/mobility, and 4) minimizing eNB/CN signaling load. All these requirements are taken into consideration and realized under the proposed HetNet architecture.

Fig. 3 shows the schematic diagram of the proposed LTE/Wi-Fi/mmWave interworking. As shown in Fig. 3, the (Wi-Fi/mmWave) WLAN is tightly integrated with the LTE at the PDCP layer, since integrating at other layers such physical (PHY) and MAC are not appropriate. The integration at the PHY would require significant standards modifications, which violates the aforementioned 3GPP recommendations. Also, the integration at the MAC layer needs the design of multi-band MAC protocols, and it would introduce synchronization challenging issues. As shown in Fig. 3, to facilitate the design of the proposed hierarchal LTE/Wi-Fi/mmWave HetNet, an LTE/WLAN protocol adaptor is proposed. This will isolate and hide the WLAN physical interfaces from the LTE upper layer, since it is used to package and translate signals from WLAN to LTE and vice versa. Fig. 3 shows that the C1-plane and C2-plane signaling are transmitted by the LTE eNB and Wi-Fi, respectively; while the real time mmWave MAC signaling e.g., mmWave BT, association request and response, etc., are performed in the mmWave band. The U-plane can be carried by either LTE, Wi-Fi or mmWave bands based on the availability.

A. MANAGEMENT PROTOCOL

As shown in Fig. 4, the management protocol of the proposed LTE/Wi-Fi/mmWave HetNet consists of two types of management operations associated with the inter sub-cloud and the intra sub-cloud statuses of the UE. The LTE eNB provides a continuous C1-plane coverage in the inter sub-cloud status of the UE. As the UE is detected to be within the coverage area of Wi-Fi/mmWave sub-clouds via LTE-based localization, offloading decision may be taken

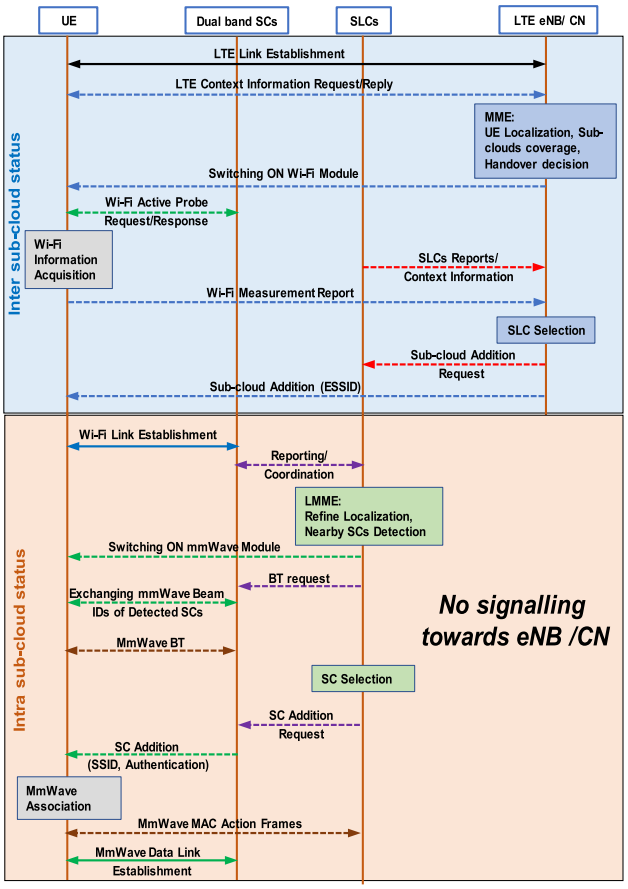

FIGURE 4. Proposed LTE/Wi-Fi/mmWave management protocol.

by LTE mobility management based on the estimated traffic loads on both LTE eNB and the detected sub-clouds and UE traffic demands. Should an offloading decision be taken, sub-cloud selection and Wi- Fi/mmWave SC association can be carried out by the aid of the collected reports from the UE and the detected SLCs as follows:

1. UE will be triggered for switching ON its Wi-Fi module if it is in a sleep mode by the LTE eNB via C1 plane. The UE ON/OFF switching based on the usage is used toefficiently reduce the consumed energy and saving the UE battery.
2. UE Wi-Fi module broadcasts active probe request frame to discover its surrounding Wi-Fi/mmWave sub-clouds using C2 plane. After receiving Wi-Fi probe response frames from the surrounding sub-clouds via the C2 plane, UE acquires their essential information, e.g., ESS identifiers (ESSIDs), signal-to-interference-plus-noise ratios (SINRs), etc.
3. UE sends the collected information to the LTE eNB via the C1 plane. Utilizing this information along with the current statuses of the detected sub-clouds including the status of their Wi-Fi and mmWave bands, reported to the LTE eNB via the backhaul links, a sub-cloud is selected by the LTE eNB for associating the UE. Then, it informs the UE by the ESSID of the selected

sub-cloud. Also, it informs the selected sub-cloud by the collected UE context information, e.g., its traffic demand, MAC address, etc.

4. Finally, UE associates with the selected sub-cloud using Wi-Fi interface via C2 plane signaling, and a Wi-Fi link is established.

In the intra sub-cloud status, the UE will be under the control of the associated SLC within a local mobility domain. Inside the sub-cloud, the interoperation between the Wi-Fi and mmWave can be summarized as follows:

1. The SLC continuously collects the Wi-Fi received signal strength (RSS) readings experienced by the UE. Then, finer UE location information can be estimated using Wi-Fi-based localization.
2. Inside the sub-cloud, the probability of mmWave coverage can be estimated utilizing the accurate UE location information. Also, exploiting UE location information can extremely relax the BT complexity by reducing the search space for the mmWave SC and UE [46].
3. If the decision is that the UE can be covered by mmWave access [46], a switch ON control frame is transmitted by the SLC to the UE via the C2 plane to switch ON its mmWave module if it is in a sleep mode. Then, information related to mmWave best beam IDs required for the BT process by the detected Wi-Fi/mmWave SCs can be carried to the UE via C2 plane.
4. Based on the collected Wi-Fi/mmWave UE measurements inside the sub-cloud, e.g., the traffic loads on the detected SCs including their Wi-Fi and mmWave bands and UE traffic demands, the SLC decides the best SC to convey the user data traffic. Then, the SLC informs the UE by the SSID of the selected SC. Also, it informs the selected SC by the collected UE context information, e.g., its traffic demand, MAC address, etc., to associate with it and steer communication session towards its mmWave link using mmWave U-plane for data traffic while maintaining Wi-Fi C2 plane for signaling.

B. U-PLANE PROTOCOL STACK

Obviously, the proposed architecture follows the current 3GPP standardization [15] without any LTE modification with respect to LTE eNB and CN as legacy LWA. The architecture only requires that IEEE standardization supports the use of dual band Wi-Fi/mmWave SCs, which is already standardized by IEEE 802.11ad [29] for backward compatibility. The aggregated U-plane path can be tracked by Fig. 5, as follows:

- User data originated from CN is transferred to serving eNB on S1 interface through general packet radio service (GPRS) tunneling protocol.
- U-plane can be served through LTE, Wi-Fi or mmWave band based on the reports collected from sub-clouds and UE.

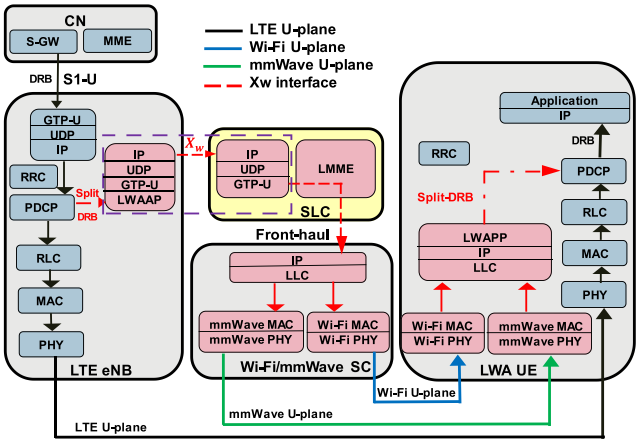

FIGURE 5. Proposed protocol stack of the U-plane.

- Using split data radio bearer (DRB) in Fig. 5, data packets at PDCP layer are scheduled for transmissions using either LTE eNB or sub-cloud.
- Standardized LWA adaptation protocol (LWAAP) [15] layer provides required adaptation/encapsulation for forwarding split data packets on WLAN. It adds DRB ID and packet ordering to allow re-ordering when aggregated at UE. As well as data is transferred from CN to LTE eNB via tunneling, it also transferred from LTE eNB to WLAN sub-cloud via tunneling over standardized Xw interface as the conventional LWA non co-located scheme [13].
- Data packets can be forwarded from SLC to the serving SC on high speed front-haul link. Switching between sub-cloud SCs (Horizontal HO) and between available air interfaces (Vertical HO) are done in the same SC under SLC control without LTE eNB involvement. In other words, IEEE-based WLAN operation is left for IEEE management under sub-cloud control.
- At UE, received data from either Wi-Fi or mmWave, will be de-capsulated, re-ordered by LWAAP layer, aggregated with normal LTE packets at PDCP, and introduced to LTE higher layers.

C. C1, C2-PLANE PROTOCOL STACK

Fig. 6 shows the detailed structure of the C1 and C2 protocol stack of the proposed HetNet, which can be explained as:

- Control signaling is divided between two control planes (C1 and C2). C1 signaling is introduced from centralized MME at CN and transmitted by LTE eNB, and C2 signaling is introduced from the distributed local MMEs (LMMEs) at SLCs and transmitted via the Wi-Fi band.
- UE is provided by two radio resource control (RRC) message translators: the first one for translating RRC messages carried by C1 for driving Wi-Fi UE module, and the second one for translating RRC messages carried by C2 for driving mmWave module of the UE.

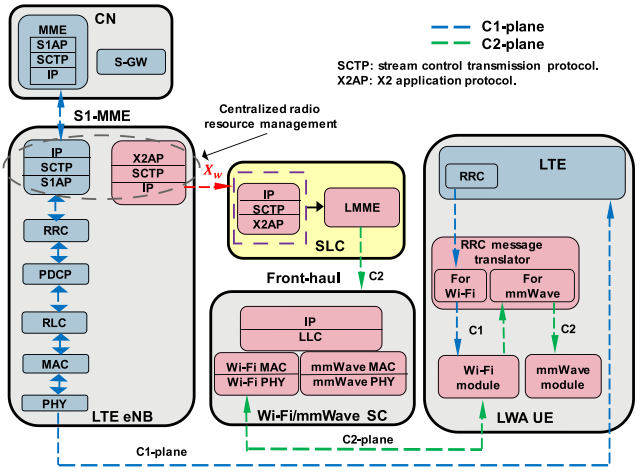

FIGURE 6. Proposed protocol stack of the C1 and C2 planes.

V. MATHEMATICAL ANALYSIS

In this section, analytical frameworks to precisely bound the performance of both the conventional LTE/mmWave and the proposed LTE/Wi-Fi/mmWave HetNets are developed. To this end, analytical models are introduced for many important and interrelated parameters to analytically assess the gains of the proposed HetNet over the conventional one in terms of mmWave band utilization, mmWave energy efficiency and eNB/CN signaling load. In this paper, the simple Markov model (MM) is used to model the steady state probabilities of the U-plane of the conventional HetNet, since the observed U planes are directly related to the LTE and mmWave states. On the other hand, due to the use of the hierarchal architecture in the proposed HetNet enabled by 2C/U plane splitting, the operation of the proposed HetNet can be efficiently modeled using hidden Markov model (HMM). In which, the 2C planes represent the hidden states of the HMM, i.e., inter sub-cloud and intra sub-cloud states. Whereas, the U planes represent the observable states, i.e., LTE, Wi-Fi or mmWave U planes. Considering that UE will be attached to the highest data rate U-plane whenever it is available; thus, as long as the LTE-U is observed, the inter sub-cloud (C1) state occurs. Similarly, as long as the Wi-Fi-U or mmWave-U are observed, the intra sub-cloud (C2) state happens.

Fig. 7 (a), shows the MM of the two different U-plane statuses in the conventional HetNet. It is assumed that the UE will be attached to the band that provides the highest data rate U-plane whenever it is available. This can be represented by the Markovien transition matrix, $\mathfrak{M}_{L/m}$, which can be expressed as:

$$\mathfrak{M}_{L/m} = \begin{pmatrix} 1 - P^m_{CT}(1-P_b) & P^m_{CT}(1-P_b) \\ 1 - P^m_a(1-P_b) & P^m_a(1-P_b) \end{pmatrix}, \quad (9)$$

where P_b represents the blocking probability of the LOS link between the mmWave SC and the UE. P^m_{CT}, represents the probability of the correct transition of the U-plane from LTE

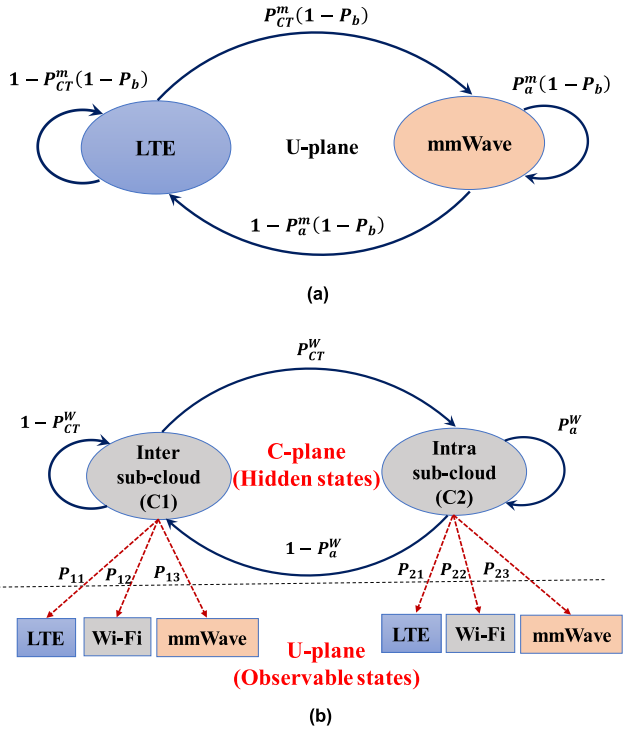

FIGURE 7. Markov models for the conventional and the proposed HetNets. (a) MM for the U-plane of the conventional LTE/mmWave HetNet. (b) HMM for the U-plane of the proposed HetNet.

to the mmWave, which can be expressed as:

$$P^m_{CT} = P^m_a\left(1 - P^C_{miss}\right), \quad (10)$$

where P^m_a is the actual availability of the mmWave band and it represents the percentage of the total mmWave coverage with respect to the LTE eNB coverage. P^C_{miss} is the miss detection probability of the mmWave band in the conventional HetNet mainly comes from the errors in LTE-based UE positioning, and it is defined as the probability that the UE is estimated to be in the *out-of-coverage* areas of the mmWave SCs; while it is actually located in their coverages. Higher values of the miss detection probability indicate higher percentages of losing the opportunity of linking the UE with the high capacity mmWave SCs, which is not desirable. More details about P^m_a and P^C_{miss} and their analytical derivations can be found in Appendices A and B, respectively.

By directly solving (9), in the steady state using (10), the mmWave and LTE U-plane probabilities, P^m_C and P^{LTE}_C, of the conventional HetNet, can be expressed as:

$$P^m_C = \frac{P^m_a\left(1 - P^C_{miss}\right)(1-P_b)}{1 - P^m_a P^C_{miss}(1-P_b)}, \quad (11)$$

$$P^{LTE}_C = 1 - P^m_C = 1 - \left(\frac{P^m_a\left(1 - P^C_{miss}\right)(1-P_b)}{1 - P^m_a P^C_{miss}(1-P_b)}\right). \quad (12)$$

On the other hand, Fig. 7 (b), shows the HMM for the U-plane of the proposed HetNet. The transition and observation matrices $\mathfrak{M}_{\text{inter/intra}}$ and $\mathcal{H}$ of the HMM of the proposed

HetNet, can be expressed as:

$$\mathfrak{M}_{\text{inter/intra}} = \begin{pmatrix} 1 - P_{CT}^{W} & P_{CT}^{W} \\ 1 - P_{a}^{W} & P_{a}^{W} \end{pmatrix}, \tag{13}$$

$$\mathfrak{H} = \begin{pmatrix} P_{11} & P_{12} & P_{13} \\ P_{21} & P_{22} & P_{23} \end{pmatrix}, \tag{14}$$

where P_{CT}^{W} represents the probability of the correct transition from the inter sub-cloud status to the intra sub-cloud status and can be formulated as:

$$P_{CT}^{W} = P_{a}^{W}\left(1 - P_{miss}^{W}\right), \tag{15}$$

where P_{a}^{W} and P_{miss}^{W} represent the actual availability and the miss detection probability of the Wi-Fi band (sub-cloud) inside the LTE coverage, see Appendices A and B. Again, higher values of P_{miss}^{W} mean higher percentages of losing the opportunity to connect to a sub-cloud. P_{ij} in the $\mathfrak{H}$ matrix represents the transition probability from status i in the C-plane to connection j in the U-plane. For example, P_{23} is the probability that mmWave U-plane is observed whenever UE is in the intra sub-cloud status, i.e., whenever C2 plane is used. Based on the assumption that the UE will use the highest available data rate U-plane, then $P_{11} = 1$, $P_{12} = P_{13} = P_{21} = 0$, while $P_{23} = \frac{P_{a}^{m}}{P_{a}^{W}}(1-P_{miss}^{P})(1-P_{b})$ and $P_{22} = 1-P_{23}$. P_{miss}^{P} is the mmWave band miss detection probability inside the sub-cloud of the proposed HetNet, which mainly comes from the errors of the Wi-Fi-based UE localization, see Appendix B. More details about P_{a}^{W}, P_{miss}^{W} and P_{miss}^{P} and their analytical derivations can be found in Appendices A and B, respectively.

By solving the Markovien transition matrix in (13) in the steady state using (15), the different C-plane probabilities, P^{intra} and P^{inter}, that the UE is within the intra sub-cloud status and controlled by C2, or within the inter sub-cloud status and controlled by C1, respectively, can be expressed as:

$$P^{\text{intra}} = \frac{P_{a}^{W}\left(1 - P_{miss}^{W}\right)}{1 - P_{a}^{W}P_{miss}^{W}}, \tag{16}$$

$$P^{\text{inter}} = 1 - P^{\text{intra}} = 1 - \left(\frac{P_{a}^{W}\left(1 - P_{miss}^{W}\right)}{1 - P_{a}^{W}P_{miss}^{W}}\right). \tag{17}$$

Consequently, using (14), the different mmWave, Wi-Fi and LTE U-plane probabilities P_{P}^{m}, P_{P}^{W} and P_{P}^{LTE} of the proposed HeNet, can be calculated as:

$$P_{P}^{m} = P^{\text{inter}}P_{13} + P^{\text{intra}}P_{23}, \tag{18}$$

$$P_{P}^{W} = P^{\text{inter}}P_{12} + P^{\text{intra}}P_{22}, \tag{19}$$

$$P_{P}^{LTE} = P^{\text{inter}}P_{11} + P^{\text{intra}}P_{21}. \tag{20}$$

Substituting from (16) and (17) and using the values of P_{ij} of the $\mathfrak{H}$ matrix, (18), (19) and (20) can be re-written as:

$$P_{P}^{m} = \frac{P_{a}^{m}\left(1 - P_{miss}^{P}\right)\left(1 - P_{miss}^{W}\right)(1 - P_{b})}{1 - P_{a}^{W}P_{miss}^{W}}, \tag{21}$$

$$P_{P}^{W} = \frac{\left[P_{a}^{W} - P_{a}^{m}\left(1 - P_{miss}^{P}\right)(1 - P_{b})\right]\left(1 - P_{miss}^{W}\right)}{1 - P_{a}^{W}P_{miss}^{W}}, \tag{22}$$

$$P_{P}^{LTE} = 1 - \left(\frac{P_{a}^{W}\left(1 - P_{miss}^{W}\right)}{1 - P_{a}^{W}P_{miss}^{W}}\right). \tag{23}$$

VI. SIMULATION ANALYSIS

In this section, the performance of the proposed LTE/Wi-Fi mmWave HetNet and the conventional LTE/mmWave HetNet like the benchmark schemes given in [37] and [38] are compared using exhaustive numerical simulations. Moreover, the accuracy of the system mathematical analysis is verified through comparisons between the results come from the mathematical framework and the numerical simulations.

A. SIMULATION SCENARIO

In the simulation scenario, the target environment is considered to be the coverage of one LTE eNB located at the center. In this macro area, fixed number of Wi-Fi/mmWave sub-clouds are overlaid to cover almost this area. In each sub-cloud, dual band SCs are implemented to provide the Wi-Fi and mmWave services. As, the network densification strategy will be the dominant theme for the 5G networks, the number of the SCs per sub-cloud is varied to evaluate the system performance under different values of SCs density. The UE is always connected with the LTE eNB. When the UE is only covered by the macro service, the C1-plane and U-plane are supported by the LTE eNB. As the UE joins a sub-cloud, all the control signaling is done by the C2-plane supported by the Wi-Fi band via the SLC, and the U-plane is opportunistically provided by the Wi-Fi or the mmWave bands based on their availabilities. The main simulation parameters and their corresponding values are listed in Table 1. During the simulation, one UE is assumed to be randomly dropped in the LTE eNB coverage and moving in a random direction with velocity v km/h during the simulation period T.

B. EVALUATION METRICS

In the following analysis, for fair comparisons and to focus on the efficient usability of the mmWave band, the HetNets performance is evaluated and compared only with respect to the mmWave band under different mmWave SCs densities. In this context, many key parameters, such as mmWave band accessibility, eNB/CN signaling load and the mmWave initial access complexity are used as performance evaluation metrics. The mmWave band accessibility has been mathematically formulated in Section V as P_{C}^{m} and P_{P}^{m} in (11) and (21) for the conventional and the proposed HetNets, respectively. In addition, as a new proposed metric, this paper introduces the mmWave usability as a measure to quantify how much the mmWave band is efficiently utilized in the HetNet with respect to average rate and energy consumption. When correctly deciding that the UE is located within the mmWave coverage based on localization, a correct HO decision may be taken if blocking is not happened. Thus, a useful mmWave link may be established with the UE, and useful mmWave

TABLE 1. Simulation parameters.

Parameter	Value
$\mathcal{P}_t^{LTE}/\mathcal{P}_t^W/\mathcal{P}_t^m$ (dBm)	46/ 20/ 10
Carrier frequency (GHz) (LTE/Wi-Fi/mmWave)	2/ 5/ 60
Bandwidth (GHz) (LTE/Wi-Fi/mmWave)	0.2/ 0.4/ 2
Macro LTE ISD	250 m
Antenna height (m) (LTE/Wi-Fi/mmWave)	25/ 3/ 3
UE antenna height	1.5 m
Noise power spectral density	-174 dBm/Hz
$\mathcal{P}_{th}^m$ / $\mathcal{P}_{th}^W$ (dBm)	-78/ -70
No. of sub-clouds	7
No. of SCs per sub-cloud	1- 8
Num. of antenna sectors of mmWave SC/ UE	91/1
$\Phi_{-3dB}/\Theta_{-3dB}$	20°/ 20°
δ (LTE/ Wi-Fi)	50m/ 2.5m
UE speed, v (km/h)	5 and 25
Blocking probability, P_b	0- 0.8
Simulation time, T	5 minutes

rate and energy consumption are utilized. On the other hand, due to localization error and shadowing effect, if the UE is wrongly detected to be within the mmWave coverage, a false HO decision is taken. As a result of the false HO decisions and blocking, mmWave band will conduct an un-useful antenna BT consuming mmWave rate and energy with no benefit. In this context, mmWave rate usability index R_U and energy usability index E_U, are generally defined as follows:

$$R_U = \frac{P^m.\Re^m}{P^m \cdot \Re^m + [(1-P_a).P_{FD}^m + P_a.P_b] \cdot \Re_C}, \quad (24)$$

$$E_U = \frac{P^m.\mathcal{P}_t^m}{P^m \cdot \mathcal{P}_t^m + [(1-P_a) \cdot P_{FD}^m + P_a \cdot P_b] \cdot \mu \cdot \mathcal{P}_t^m}, \quad (25)$$

where, $P^m = P_C^m$ in (11) or P_P^m in (21) for the conventional and the proposed HetNets, respectively. Also,$P_a = P_a^m$ or (P_a^m/P_a^W) for the conventional and the proposed HetNets, respectively. $\Re^m$ and $\Re_C$ are the average achievable data rate and BT rate of the mmWave band, respectively. For simplicity, we assume that $\Re_C = \Re^m$, and $\mu = T_{BT}/T_f = 0.1$ is the BT time to the total frame time. P_{FD}^m is the mmWave false detection probability that the UE is estimated to be in the mmWave band coverage; while it is actually located out of its coverage. Here, P_{FD}^m can be expressed as P_{FD}^C and P_{FD}^P for the conventional and the proposed HetNets, respectively. More details about the false detection probability and its analytical formulations can be found in Appendix B. In (24) and (25), the terms in the numerators indicate the useful utilization of the mmWave band. Whereas, the terms $[(1-P_a) \cdot P_{FD}^m + P_a \cdot P_b] \cdot R_C$ and $[(1-P_a) \cdot P_{FD}^m + P_a \cdot P_b] \cdot \mu \cdot \mathcal{P}_t^m$ in the dominators indicate the un-useful utilizations of the mmWave band due to redundant BT.

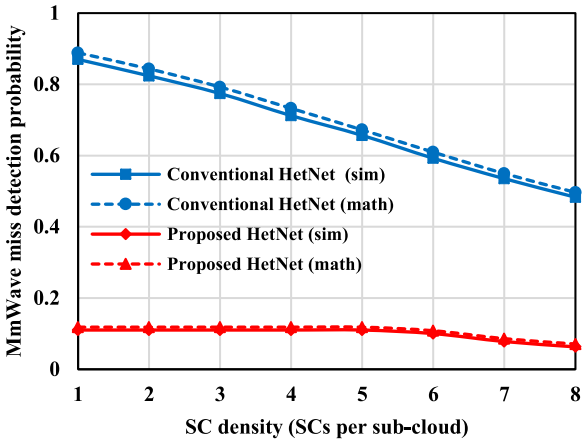

FIGURE 8. MmWave miss detection probability.

C. SIMULATION RESULTS

1) mmWave ACCESSIBILITY

Generally, as indicated in Section V, the mmWave accessibility highly depends on the mmWave miss detection probability as given in (11) and (21) for the conventional HetNet and the proposed one. Fig. 8 shows P_{miss}^C and P_{miss}^P obtained by the mathematical models given in Appendix B and the numerical simulations for the conventional and the proposed HetNets against different mmWave SCs densities at $v = 5$ km/h, respectively. Here, P_{miss}^C is calculated for the conventional HetNet with respect to the LTE eNB coverage, while, P_{miss}^P is calculated per sub-cloud and averaged over all sub-cloud in the proposed HetNet. Clearly, P_{miss}^P calculated over the sub-clouds is comparable to P_{miss}^C calculated over the whole LTE eNB area because the mmWave service is only available in the sub-cloud area. From Fig. 8, as the number of deployed mmWave SCs is increased the mmWave miss detection probability is decreased. Also, the conventional HetNet has higher mmWave miss detection probability due to the higher LTE localization error compared to the coverage area of the mmWave SC. On the other hand, the proposed HetNet has lower Wi-Fi and mmWave miss detection probabilities. A constant $P_{miss}^W = 0.26$ is achieved in the proposed HetNet due to the use of a fixed number of deployed sub-clouds in the LTE eNB area. Also, using 5 SCs/sub-cloud, 82% reduction in mmWave miss detection probability is obtained using the proposed HetNet over the conventional one. These results are achieved thanks to the proposed two stage UE localization process; in which an LTE-based localization is used to localize the UE in accordance to the wide coverage sub-clouds, and the accurate Wi-Fi-based localization is used to localize it against the small coverage mmWave SCs.

The effect of the miss detection probability on the mmWave accessibility is shown in Fig. 9. This figure shows the mmWave actual availability, P_a^m, and the mmWave band accessibilities, P_C^m and P_P^m at $v = 5$ km/h, respectively without

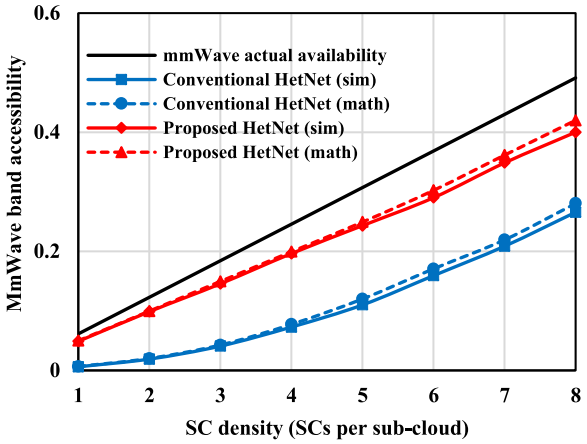

FIGURE 9. MmWave band accessibility, $P_b = 0$.

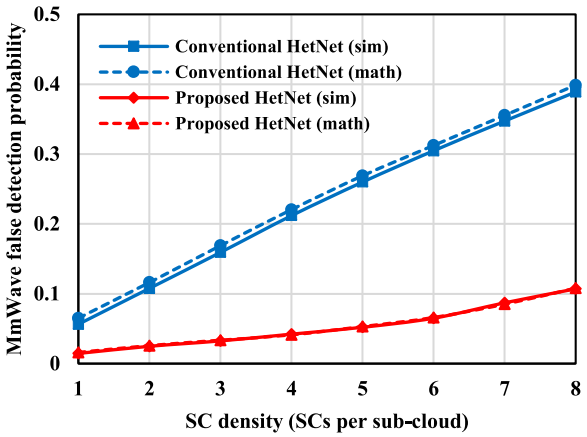

FIGURE 10. MmWave false detection probability.

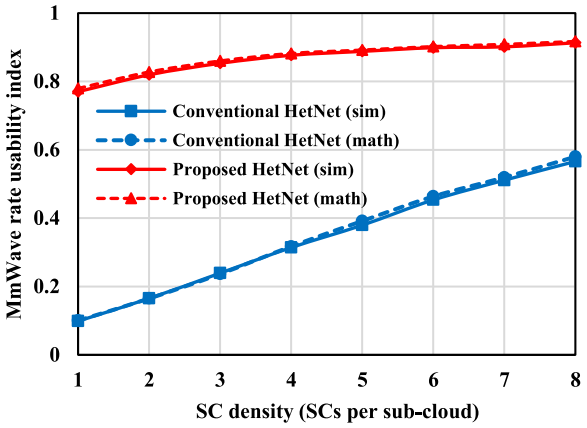

FIGURE 11. MmWave rate usability, $P_b = 0$.

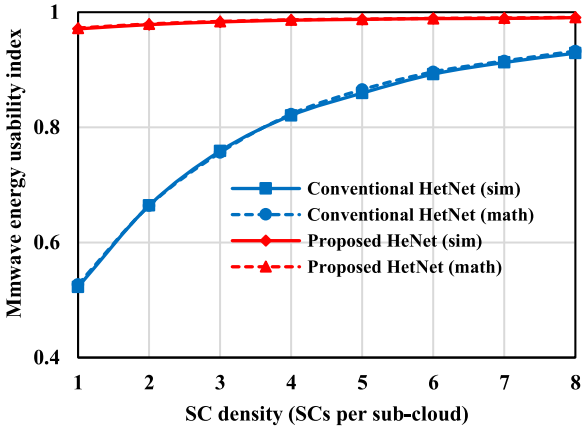

FIGURE 12. MmWave energy usability, $P_b = 0$.

considering the blocking effect, i.e. $P_b = 0$. The results obtained by the mathematical Markovien models given in (11) and (21) and those obtained by the numerical simulations are approximately matched. Also, the proposed HetNet efficiently accesses the available mmWave band since P_P^m nearly reaches P_a^m. Yet, P_C^m of the conventional HetNet is significantly far from P_a^m, which indicates poor mmWave accessibility. For example, with 5 SCs per sub-cloud, the proposed HetNet outperforms the conventional one by about 50% in the mmWave band accessibility.

2) mmWave RATE AND ENERGY USABILITY WITHOUT BLOCKING EFFECT

As given in (24) and (25), both R_U and E_U are inversely proportional to P_{FD}^m. Thus, P_{FD}^C and P_{FD}^P are calculated for the conventional and the proposed HetNets, respectively based on the mathematical formulations given in Appendix B. Fig. 10 shows the false detection probabilities obtained by the mathematical models given in Appendix B and that obtained using numerical simulations for the proposed and the conventional HetNet against mmWave SCs density at $v = 5$ km/h. Generally, the mmWave false detection probability is increased with increasing the density of mmWave SCs due to the increase in the erroneous in mmWave coverage decisions. Also, the proposed HetNet outperforms the conventional one in terms of mmWave false detection probability at all tested SCs densities. At 5 SCs per sub-cloud, about 80% reduction in mmWave false detection probability is obtained using the proposed HetNet.

Fig. 11 and Fig. 12 give R_U and E_U of the compared HetNets using both the mathematical models and the numerical simulations against mmWave SCs density at $v = 5$ km/h without considering the blocking effect, i.e. $P_b = 0$. Obviously, these figures show that the proposed HeNet highly utilizes the mmWave band more than the conventional one especially in low dense SCs scenarios. For example, with 3 mmWave SCs per sub-cloud, the proposed HetNet outperforms the conventional one by about 73% and 23% in R_U and E_U, respectively. This high mmWave band utilization comes from increasing P_P^m over P_C^m in addition to decreasing P_{FD}^P over P_{FD}^C owing to the use of the precise control and localization provided by the added Wi-Fi band.

3) mmWave RATE AND ENERGY USABILITY WITH BLOCKING EFFECT

Figs. 13 and 14 show R_U and E_U of the compared HetNets against different values of LOS blockage probability, P_b,

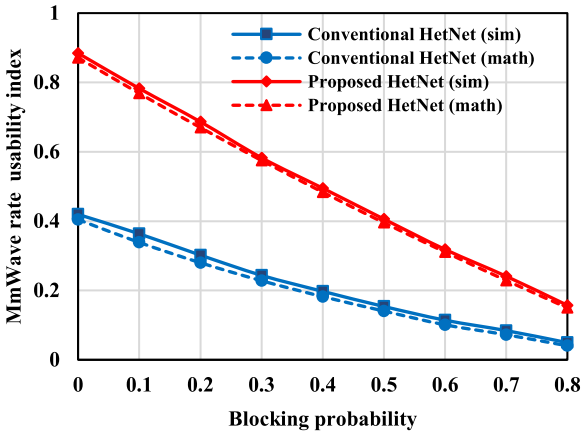

FIGURE 13. MmWave rate usability with blocking effect.

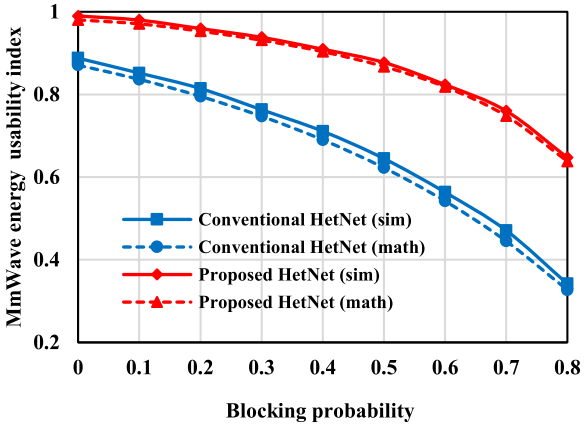

FIGURE 14. MmWave energy usability with blocking effect.

with 5 SCs per sub-cloud and at $v = 5$ km/h. Generally, the R_U and E_U are decreased with increasing P_b for both the proposed and the conventional HetNets. This is due to the fact that the blocking is significantly affect the mmWave communication and limits its accessibility. From Figs. 13 and 14, the proposed HetNet outperforms the conventional one in terms of R_U and E_U for all tested P_b values. For example, at $P_b = 0.4$, the proposed HetNet outperforms the conventional one by about 62% and 21% in R_U and E_U, respectively.

4) eNB/CN SIGNALING LOAD

In the conventional LTE/mmWave HetNet, even if a UE is moving with low or moderate speeds causes frequent HOs among the deployed mmWave SCs. This is due to the limited coverage of the mmWave SCs. In turns, a significant mobility signaling load is applied on both lte eNB and CN. Nevertheless, in the proposed HetNet, two types of HOs exist: the inter sub-cloud HO and the intra sub-cloud HO. The first HO type is needed to perform a HO between LTE eNB and the distributed sub-clouds, which requires C and U planes HOs. The second type is related to the U-plane HO among the SCs inside the sub-cloud, and it is the dominant HO type, especially in dense SCs scenario. It is assumed that each

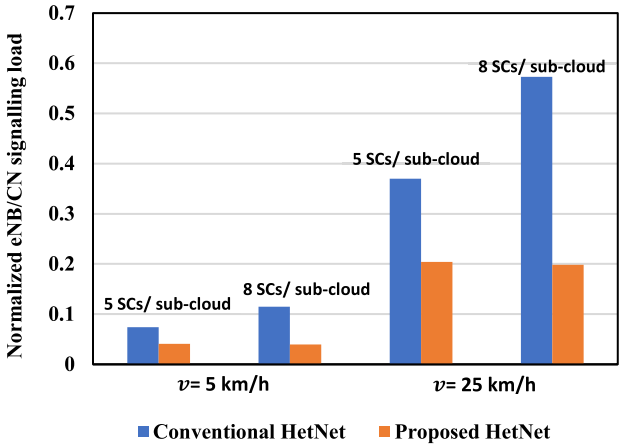

FIGURE 15. Normalized eNB/CN signaling load.

HO in the conventional HetNet and each inter sub-cloud HO in the proposed HetNet generates an equal signaling load on the eNB/CN. Since the intra sub-cloud HO in the proposed HetNet is loaded on the SLC, it does not generate any signaling load towards the eNB/CN. Thus, the total number of HOs in the conventional HetNet and the inter sub-cloud HOs in the case of the proposed HetNet per second are used to indicate the normalized signaling load on the eNB/CN. Fig. 15 shows the simulated normalized eNB/CN signaling load for the conventional and the proposed HetNets for semi-dense (5 SCs per sub-cloud) and dense SCs (8 SCs per sub-cloud) deployments at different UE speeds. Generally, as the UE speed increases, the signaling load on the eNB/CN is increased due the increasing rate of HO decisions. From Fig. 15, due to the proposed distributed control, the proposed HetNet extremely relieves the mobility signaling load on the eNB/CN especially in the dense SCs scenario at both low and moderate UE speeds. For example, with 5 (8) SCs per sub-cloud, the proposed HetNet reduces the eNB/CN signaling load by 46% (64%) over the conventional one, respectively, at both $v = 5$ km/s and 25 km/h. The high reduction in the eNB/CN signaling load comes due to the fact that, only the mobility signaling for the relatively low rate inter sub-cloud HOs is loaded on the eNB/CN, while the heavy intra sub-cloud mobility signaling is dealt by the SLC in a local domain. In contrast, in the conventional HetNet all the mobility signaling associated to HOs between the mmWave SCs is loaded on the eNB/CN.

5) mmWave INITIAL ACCESS COMPLIXITY

In this paper, the complexity of mmWave initial access is evaluated as the number of beam switchings required for establishing the mmWave link with the UE. For the proposed HetNet, we use the mmWave initial access methodology given in [31] and explained in Section III.B. For the conventional HetNet, the UE location is estimated using the LTE-based localization, and the mmWave SCs localized around the estimated UE location are directed to perform exhaustive search BT as given in [47]. Fig. 16 shows the

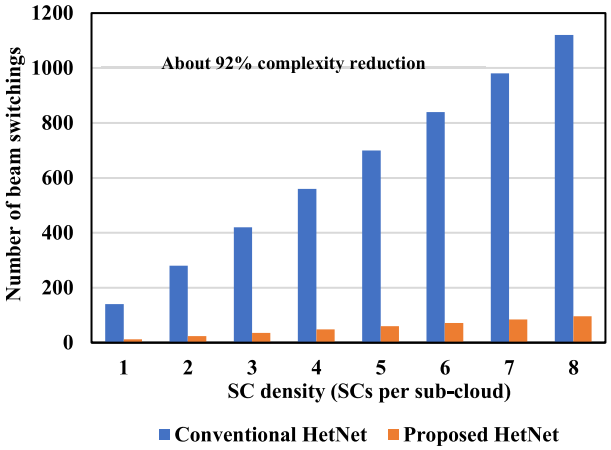

FIGURE 16. MmWave initial access complexity.

simulated number of beam switchings of the mmWave initial access for both the conventional and the proposed HetNets using different SCs densities. As shown in Fig. 16, the proposed HetNet significantly reduces the complexity of mmWave initial access over the conventional one, by 92% for all tested SCs densities. This complexity reduction is due to the accurate Wi-Fi localization compared to the LTE localization, which cannot be efficient in the SC and beam levels due to the large localization error compared to the SC and the beam coverages. Thus, in the conventional HetNet, a large number of mmWave SCs are directed to perform exhaustive search BT with the UE for initial access. However, in the proposed HetNet, only a few number of SCs with a low number of beams are used for initial access.

VII. CONCLUSION

In this paper, the complementary features of LTE, Wi-Fi and mmWave bands are proficiently leveraged to introduce a tightly coupled LTE/Wi-Fi/mmWave multi-band HetNet for 5G cellular networks. Interoperation among the different elements of the proposed HetNet is accomplished via a novel concept of 2C/U plane splitting. The detailed network architecture and the required protocol stacks of the proposed HetNet in addition to the protocol that organizes its internal operation were introduced. A rigorous mathematical framework is introduced to mathematically tight the performance for the proposed HetNet against its key parameters. Generally, simulation and mathematical results, which nearly match each other, show that the proposed HetNet significantly outperforms the conventional one which directly integrates the mmWave to the LTE via the concept of C/U splitting. Specifically, the analysis shows that the proposed HetNet has lower mmWave miss and false detection probabilities than the conventional one enabling efficient accessibility and utilization of the mmWave band. Moreover, thanks to the proposed SLC, the mobility signaling load on the eNB/CN and the mmWave associated signaling such as mmWave initial access are extremely relaxed and become transparent to the LTE eNB.

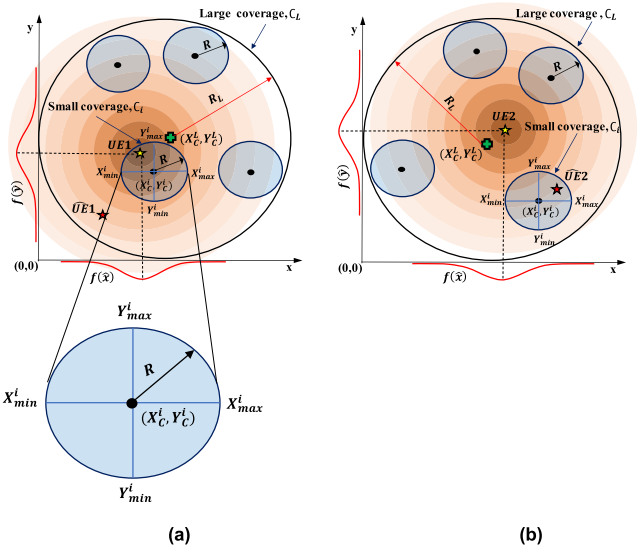

FIGURE 17. An illustration example for (a) miss detection probability and (b) false detection probability.

APPENDIX A
ACTUAL AVAILABILITYIES OF mmWave AND Wi-Fi BANDS

As defined previously, the actual availabilities of the mmWave and Wi-Fi bands, P_a^m and P_a^W, represent the percentage of the total mmWave and Wi-Fi potential coverage with respect to the LTE eNB coverage, respectively. For simplicity, we assume non-overlapped coverage mmWave SCs and Wi-Fi sub-clouds, and the sub-cloud coverage is defined only by the Wi-Fi SC located at its center. Thus, potential path loss models given in Section III, averaged over the shadowing term, can be used for evaluating P_a^m and P_a^W. The potential coverage of an mmWave SC or a Wi-Fi sub-cloud is bounded by its potential range R. Here, R represents the maximum distance from an mmWave SC (Wi-Fi sub-cloud) center of coverage; where the received power by a UE exceeds the receiver sensitivity threshold, $\mathcal{P}_{th}^m$ ($\mathcal{P}_{th}^W$), respectively. For example, the small coverage, C_i in Fig. 17 (a) and (b), represents the potential coverage of an SC (sub-cloud) with a potential transmission range R, which can be obtained based on the potential pathloss models given at Section III. According to this definition, P_a^m and P_a^W for the mmWave and Wi-Fi bands inside the LTE eNB coverage, using (5) and (3) and assuming LOS condition for mmWave, can be expressed as:

$$P_a^m = \frac{\pi N^m \left(d_0^m 10^{\left(\mathcal{P}_t^m + G_{m\mathrm{dB}} - \mathcal{P}_{th}^m - 82.02\right)/(38.8)} \right)^2}{A_c^{LTE}}, \tag{26}$$

$$P_a^W = \frac{\pi N^W \left(d_0^W 10^{\left(\mathcal{P}_t^W - \mathcal{P}_{th}^W - 47.2\right)/(23.2)} \right)^2}{A_c^{LTE}}, \tag{27}$$

where N^m and N^W represent the total number of deployed mmWave SCs and Wi-Fi sub-clouds in the LTE

eNB coverage, respectively. A_c^{LTE} is the LTE eNB coverage area based on the inter-site distance (ISD).

APPENDIX B
MISS AND FALSE DETCTION PROBABILITIES

As previously mentioned, P_{miss}^{W} and P_{miss}^{m} are the probabilities that the UE is estimated to be in the *out-of-coverage* areas of the Wi-Fi sub-clouds and the mmWave SCs; while it is actually located in their coverages, respectively. By analogy, the false detection probabilities P_{FD}^{W} and P_{FD}^{m} are the probabilities that the UE is estimated to be in the sub-clouds and the mmWave SCs coverage; while it is actually located out of their coverages, respectively. The UE localization accuracy highly effects the miss and false detection probabilities; hence, higher localization accuracy results in lower values of miss and false detection probabilities and vice versa. Lower values of the miss detection and the false detection probabilities are highly desirable as they indicate lower percentages of losing the opportunities to link with the high capacity SCs and redundant scanning for SCs connectivity, respectively.

The following mathematical analysis is general and can be applied for evaluating the miss detection and the false detection probabilities of both mmWave SCs and Wi-Fi sub-clouds. For illustration purposes, Fig. 17 (a) and (b) show a graphical representation of the miss and the false detection probabilities, respectively. In Fig. 17 (a) and (b), the large coverage, C_L represents either the LTE eNB or a Wi-Fi sub-cloud coverage, and the small coverage, C_i represents either a mmWave SC or a Wi-Fi sub-cloud coverage. As an illustration example for the miss detection probability, in Fig. 17 (a), $UE1$ is actually located in the coverage of C_i, but it is wrongly estimated to be $\widehat{UE}1$, which is in the *out-of-coverage* areas of $\forall_i$. Accordingly, $UE1$ will miss the opportunity to get the high resources available in C_i because the SLC (LTE eNB) will not request the UE to switch ON it mmWave (Wi-Fi) module and start scanning for mmWave (Wi-Fi) connectivity, respectively. Thus, the miss detection probability, $P_{miss}^{\mathrm{C}_i}$ for a certain actual location $UE(x, y)$ and its estimated location $\widehat{UE}(\hat{x}, \hat{y})$, where x, y and $\hat{x}, \hat{y}$ are the actual and estimated x and y positions of the UE, can be expressed as:

$$P_{miss}^{\mathrm{C}_i} = P\left(\widehat{UE}(\hat{x}, \hat{y}) \notin \forall \mathrm{C}_i | UE(x, y) \in \mathrm{C}_i\right), \quad 1 \le i \le N \tag{28}$$

where N is the total number of the distributed C_is, i.e., mmWave SCs or sub-clouds. Specifically, while calculating P_{miss}^{W} and P_{miss}^{P} in the proposed HetNet, N is considered as the total number of the deployed Wi-Fi sub-clouds in the LTE eNB coverage and the total number of the deployed mmWave SCs in a Wi-Fi sub-cloud coverage, respectively. On the other hand, while calculating P_{miss}^{C}, N is considered as the total number of the deployed mmWave SCs in the LTE eNB coverage.

The description of the coverage C_i is illustrated in detail in Fig. 17, which is considered as a planer circular disk in the UE horizontal plane with a radius R centered at (X_C^i, Y_C^i). As shown in Fig. 17, the minimum and the maximum boundaries of C_i in the x and y directions $X_{min}^i, X_{max}^i, Y_{min}^i$ and Y_{max}^i, respectively, can be expressed in terms of R, X_C^i and Y_C^i, as follows:

$$X_{min}^i = X_C^i - R, X_{max}^i = X_C^i + R, \tag{29}$$
$$Y_{min}^i = Y_C^i - R, Y_{max}^i = Y_C^i + R. \tag{30}$$

Thus, the planer disk region, C_i, can be mathematically expressed in terms of R, X_C^i and Y_C^i as follows:

$$\mathrm{C}_i := \left\{(x, y) : \left(x - X_C^i\right)^2 + \left(y - Y_C^i\right)^2 \le R^2\right\},$$
$$X_{min}^i \le x \le X_{max}^i, \quad Y_{min}^i \le y \le Y_{max}^i, \tag{31}$$

Based on the equality condition in (31), the boundaries of y for a specific value of x, can be expressed as:

$$y(x) = Y_C^i \pm \sqrt{R^2 - \left(x - X_C^i\right)^2}. \tag{32}$$

The estimated UE position, $\hat{x}$ and $\hat{y}$ are modeled as two independent Gaussian random variables with mean values given by the actual UE position, x and y, respectively, and with standard deviation, δ [48]. Hence, as indicated in Fig. 17 (a), the probability distribution functions (PDFs), $f\left(\hat{x}\right)$ and $f\left(\hat{y}\right)$ are independent with joint PDF of:

$$f\left(\hat{x}, \hat{y}\right) = f\left(\hat{x}\right) f\left(\hat{y}\right) = \frac{1}{2\pi\delta^2} e^{\frac{-(\hat{x}-x)^2}{2\delta^2}} e^{\frac{-(\hat{y}-y)^2}{2\delta^2}}. \tag{33}$$

From Fig. 17 (a) and using (33), (28) can be expressed as:

$$P_{miss}^{\mathrm{C}_i} = 1 - \left(\sum_{i=1}^{N} \iint_{\mathrm{C}_i} f\left(\hat{x}, \hat{y}\right) d\hat{x} d\hat{y}\right), \quad x, y \in \mathrm{C}_i \tag{34}$$
$$= 1 - \left(\frac{1}{2\pi\delta^2} \sum_{i=1}^{N} \iint_{\mathrm{C}_i} e^{\frac{-(\hat{x}-x)^2}{2\delta^2}} e^{\frac{-(\hat{y}-y)^2}{2\delta^2}} d\hat{x} d\hat{y}\right). \quad x, y \in \mathrm{C}_i \tag{35}$$

Thus, the miss detection probability over all UE locations and the coverages of the $N\mathrm{C}_i$s, i.e., mmWave SCs or sub-clouds, P_{miss} can be formulated as:

$$P_{miss} = \frac{1}{N}\left[\sum_{k=1}^{N} \frac{1}{A_{C_k}} \iint_{\mathrm{C}_k} \left(1 - \sum_{i=1}^{N} \frac{1}{2\pi\delta^2} \times \iint_{\mathrm{C}_i} e^{\frac{-(\hat{x}-x)^2}{2\delta^2}} e^{\frac{-(\hat{y}-y)^2}{2\delta^2}} d\hat{x} d\hat{y}\right) dxdy\right], \tag{36}$$

where, A_{C_k} represents the area covered by the k^{th} SC (sub-cloud). By substituting from (31) and (32) into (36), P_{miss} can be finally expressed as in (37), as shown at the top of the net page. (37) can be used to evaluate P_{miss}^{C} given in (11) of the conventional HetNet, by using δ^2 of the LTE localization and C_i, N corresponding to the distributed mmWave SCs in the LTE eNB area. Moreover, it can be used to evaluate P_{miss}^{P} and P_{miss}^{W} of the proposed HetNet, by using δ^2 of the

$$P_{miss} = \frac{1}{N}\left[\sum_{k=1}^{N}\frac{1}{A_{C_k}}\int_{x=X_C^k-R}^{X_C^k+R}\int_{y=Y_C^k-\sqrt{R^2-\left(x-X_C^k\right)^2}}^{Y_C^k+\sqrt{R^2-\left(x-X_C^k\right)^2}} \times\left(1-\sum_{i=1}^{N}\frac{1}{2\pi\delta^2}\int_{\hat{x}=X_C^i-R}^{X_C^i+R}\int_{\hat{y}=Y_C^i-\sqrt{R^2-\left(\hat{x}-X_C^i\right)^2}}^{Y_C^i+\sqrt{R^2-\left(\hat{x}-X_C^i\right)^2}} e^{\frac{-(\hat{x}-x)^2}{2\delta^2}} e^{\frac{-(\hat{y}-y)^2}{2\delta^2}} d\hat{x}d\hat{y}\right) dxdy\right]. \quad (37)$$

$$P_{FD} = \frac{1}{A_c^L}\left[\int_{x=X_C^L-R_L, x\notin\forall_i}^{X_C^L+R_L}\int_{y=Y_C^L-\sqrt{R_L^2-\left(x-X_C^L\right)^2}, y\notin\forall_i}^{Y_C^L+\sqrt{R_L^2-\left(x-X_C^L\right)^2}} \times\left(\sum_{i=1}^{N}\frac{1}{2\pi\delta^2}\int_{\hat{x}=X_C^i-R}^{X_C^i+R}\int_{\hat{y}=Y_C^i-\sqrt{R^2-\left(\hat{x}-X_C^i\right)^2}}^{Y_C^i+\sqrt{R^2-\left(\hat{x}-X_C^i\right)^2}} e^{\frac{-(\hat{x}-x)^2}{2\delta^2}} e^{\frac{-(\hat{y}-y)^2}{2\delta^2}} d\hat{x}d\hat{y}\right) dxdy\right]. \quad (41)$$

Wi-Fi localization and LTE localization along with C_i, N corresponding to the distributed mmWave SCs and sub-clouds in the sub-cloud and LTE eNB areas, respectively.

Fig. 17 (b) illustrates an example explaining the concept of the false detection probability. In this example $UE2$ is actually in the *out-of-coverage* areas of $\forall C_i$, i.e., mmWave SCs or sub-clouds, but it is wrongly estimated to be $\widehat{UE}2$, which is in the coverage of C_i. This causes redundant C_i scanning, which highly consumes the UE battery without benefit. The false detection probability, $P_{FD}^{C_i}$ for a certain actual location $UE(x, y)$ and its estimated location $\widehat{UE}(\hat{x}, \hat{y})$ can be expressed as follows:

$$P_{FD}^{C_i} = P\left(\widehat{UE}(\hat{x}, \hat{y}) \in C_i | UE(x, y) \notin \forall C_i\right). \quad (38)$$

Using Fig. 17 (b) and (33), (38) can be re-written as:

$$P_{FD}^{C_i} = \sum_{i=1}^{N}\iint_{C_i} f\left(\hat{x}, \hat{y}\right) d\hat{x}d\hat{y}. \quad x, y \notin \forall C_i \quad (39)$$

By adopting the same procedure used to deduce the miss detection probability, the false detection probability P_{FD} over the whole actual UE locations in the *out-of-coverage* areas of $\forall C_i$, can be formulated as:

$$P_{FD} = \frac{1}{A_c^L}\left[\iint_{C_{L,x,y\notin\forall_i}}\left(\sum_{i=1}^{N}\frac{1}{2\pi\delta^2} \times\iint_{C_i} e^{\frac{-(\hat{x}-x)^2}{2\delta^2}} e^{\frac{-(\hat{y}-y)^2}{2\delta^2}} d\hat{x}d\hat{y}\right) dxdy\right], \quad (40)$$

A_c^L represents the area of the large coverage, C_L. In defining C_L, (29) - (32) are applicable except that X_C^L, Y_C^L, R_L, X_{min}^L, X_{max}^L, Y_{min}^L, Y_{max}^L are used instead of X_C^i, Y_C^i, R, X_{min}^i, X_{max}^i, Y_{min}^i, Y_{max}^i, respectively. As shown in Fig. 17, (X_C^L, Y_C^L) and R_L represent the center and the radius of the large coverage area, C_L, respectively. X_{min}^L, X_{max}^L, Y_{min}^L, Y_{max}^L are minimum and maximum boundaries of C_L in the x and y directions. Likewise, P_{miss} given in (37), P_{FD} can be finally expressed as given in (41), as shown at the top of the this page. Also, P_{FD} is a general equation that can be used for evaluating the false detection probability of the mmWave SCs in the conventional HetNet, i.e., P_{FD}^C, and the false detection probabilities of the mmWave SCs and the sub-clouds, i.e., P_{FD}^P and P_{FD}^W, in the proposed HetNet, as previously explained in the case of P_{miss}.

REFERENCES

[1] A. Alnoman and A. Anpalagan, "Towards the fulfillment of 5G network requirements: Technologies and challenges," *Telecommun. Syst.*, vol. 65, pp. 101–116, May 2017.

[2] X. Ge, S. Tu, G. Mao, and C. X. Wang, "5G ultra-dense cellular networks," *IEEE Trans. Wireless Commun.*, vol. 23, no. 1, pp. 72–79, Feb. 2016.

[3] P. Marsch *et al.*, "5G radio access network architecture: Design guidelines and key considerations," *IEEE Commun. Mag.*, vol. 54, no. 11, pp. 24–32, Nov. 2016.

[4] *E-UTRA and E-UTRAN; Overall Description*, document TS 36.300 (v12.1.0), 3GPP, Mar. 2014.

[5] *Information Technology–Telecommunications and Information Exchange Between Systems Local and Metropolitan Area Networks–Specific Requirements—Part 11: Wireless LAN Medium Access Control (MAC) and Physical Layer (PHY) Specifications*, IEEE Standard 802.11, ISO, 1999.

[6] Z. Yan, W. Zhou, S. Chen, and H. Liu, "Modeling and analysis of two-tier HetNets with cognitive small cells," *IEEE Access*, vol. 5, pp. 2904–2912, 2017.

[7] J. Hoadley and P. Maveddat, "Enabling small cell deployment with HetNet," *IEEE Wireless Commun.*, vol. 19, no. 2, pp. 4–5, Apr. 2012.

[8] E. M. Mohamed, "Cloud cooperated heterogeneous cellular networks for delayed offloading using millimeter wave gates," *Int. J. Electron. Telecommun.*, vol. 63, no. 1, pp. 51–64, 2017.

[9] *Part 11: Wireless LAN Medium Access Control and Physical Layer Specifications, Amendment 9: Interworking With External Networks*, IEEE Standard 802.11u, Feb. 2011.

[10] H. Park, H. H. Lee, and H. A. Chan, "Gateway service for integration of heterogeneous networks using different interworking solutions," in *Proc. 15th Int. Conf. Adv. Commun. Technol. (ICACT)*, Jan. 2013, pp. 489–494.

[11] *Access Network Discovery and Selection Function Management Object*, document TS 24.312 (v12.5.0), 3GPP, Jun. 2014.

[12] *WiMAX Forum Network Architecture Architecture, Detailed Protocols and Procedures Single Radio Interworking Between Non-WiMAX and WiMAX Access Networks*, document WMF-T37-011-R016v01, Nov. 2010.

[13] "Integration of cellular and Wi-Fi networks," 4G Americas, White Paper, Sep. 2013. [Online]. Available: https://www.ietf.org/mail-archive/web/mif/current/pdfczA7kl0W3X.pdf

[14] *Requirements and Architectures for Internet Working Between HIPERLAN/2 and 3rd Generation Cellular Systems*, document ETSI TR 101 957, ETSI, 2001.

[15] *Evolved Universal Terrestrial Radio Access (E-UTRA) and Evolved Universal Terrestrial Radio Access Network (E-UTRAN); Overall Description*, document TS 36.300 (v13.3.0), 3GPP, Apr. 2016.

[16] *Study on Wireless Local Area Network (WLAN)—3GPP Radio Interworking*, document TR 37.834 (v12.0.0), 3GPP, Dec. 2013.

[17] *Technical Specification Group Radio Access Network; Study on Small Cell Enhancement for (E-UTRA) and (e-TRAN); Higher Layer Aspects*, document TR 36.842, 3GPP, 2013.

[18] A. Zakrzewska, D. López-Pérez, S. Kucera, and H. Claussen, "Dual connectivity in LTE HetNets with split control- and user-plane," in *Proc. IEEE Globecom Workshops (GC Wkshps)*, Dec. 2013, pp. 391–396.
[19] J. G. Andrews, T. Bai, M. N. Kulkarni, A. Alkhateeb, A. K. Gupta, and R. W. Heath, Jr., "Modeling and analyzing millimeter wave cellular systems," *IEEE Trans. Commun.*, vol. 65, no. 1, pp. 403–430, Jan. 2017.
[20] T. S. Rappaport, F. Gutierrez, Jr., E. Ben-Dor, J. N. Murdock, Y. Qiao, and J. I. Tamir, "Broadband millimeter-wave propagation measurements and models using adaptive-beam antennas for outdoor urban cellular communications," *IEEE Trans. Antennas Propag.*, vol. 61, no. 4, pp. 1850–1859, Apr. 2013.
[21] K. Sakaguchi *et al.*, "Millimeter-wave wireless LAN and its extension toward 5G heterogeneous networks," *IEICE Trans. Commun.*, vol. 98, no. 10, pp. 1932–1948, 2015.
[22] W. Roh *et al.*, "Millimeter-wave beamforming as an enabling technology for 5G cellular communications: Theoretical feasibility and prototype results," *IEEE Commun. Mag.*, vol. 52, no. 2, pp. 106–113, Feb. 2014.
[23] S. Aust, R. V. Prasad, and I. G. M. M. Niemegeers, "Outdoor long-range WLANs: A lesson for IEEE 802.11ah," *IEEE Commun. Surveys Tuts.*, vol. 17, no. 3, pp. 1761–1775, 3rd Quart., 2015.
[24] G. R. Maccartney, T. S. Rappaport, M. K. Samimi, and S. Sun, "Millimeter-wave omnidirectional path loss data for small cell 5G channel modeling," *IEEE Access*, vol. 3, pp. 1573–1580, Sep. 2015.
[25] K. Hosoya *et al.*, "Multiple sector ID capture (MIDC): A novel beamforming technique for 60-GHz band multi-Gbps WLAN/PAN systems," *IEEE Trans. Antennas Propag.*, vol. 63, no. 1, pp. 81–96, Jan. 2015.
[26] N. Bhushan *et al.*, "Network densification: The dominant theme for wireless evolution into 5G," *IEEE Commun. Mag.*, vol. 52, no. 2, pp. 82–89, Feb. 2014.
[27] I. F. Akyildiz, S. Nie, S.-C. Lin, and M. Chandrasekaran, "5G roadmap: 10 key enabling technologies," *Comput. Netw.*, vol. 106, pp. 17–48, Sep. 2016.
[28] X. Ge, H. Cheng, M. Guizani, and T. Han, "5G wireless backhaul networks: Challenges and research advances," *IEEE Netw.*, vol. 28, no. 6, pp. 6–11, Nov./Dec. 2014.
[29] *Enhancements for Very High Throughput in the 60 GHz Band*, IEEE Standard 802.11ad, Dec. 2012.
[30] E. M. Mohamed, K. Sakaguchi, and S. Sampei, "Wi-Fi coordinated WiGig concurrent transmissions in random access scenarios," *IEEE Trans. Veh. Technol.*, vol. 66, no. 11, pp. 10357–10371, Nov. 2017.
[31] A. S. A. Mubarak, E. M. Mohamed, and H. Esmaiel, "Millimeter wave beamforming training, discovery and association using WiFi positioning in outdoor urban environment," in *Proc. 28th Int. Conf. Microelectron. (ICM)*, Dec. 2016, pp. 221–224.
[32] A. S. A. Mubarak, E. M. Mohamed, and H. Esmaiel, "Tightly coupled LTE/Wi-Fi/mmWave HetNet using 2C/U plane splitting for 5G networks," in *Proc. IEEE Wireless Commun. Netw. Conf. (WCNC)*, Apr. 2018, pp. 1–6.
[33] *Requirements on 3GPP System to Wireless Local Area Network (WLAN) Interworking*, document TS 22.234 (v6.0.0), 3GPP, Mar. 2004.
[34] *Technical Specification Group Services and System Aspects; Support of Optimal Routeing (SOR)*, document TS 22.079 (V9.0.0), 3GPP, Dec. 2009.
[35] O. Semiari, W. Saad, and M. Bennis, "Joint millimeter wave and microwave resources allocation in cellular networks with dual-mode base stations," *IEEE Wireless Commun.*, vol. 16, no. 7, pp. 4802–4816, Jul. 2017.
[36] O. Semiari, W. Saad, M. Bennis, and M. Debbah. (2018). "Integrated millimeter wave and sub-6 GHz wireless networks: A roadmap for ultra-reliable low-latency communications." [Online]. Available: https://arxiv.org/abs/1802.03837
[37] Q. C. Li, H. Niu, G. Wu, and R. Q. Hu, "Anchor-booster based heterogeneous networks with mmWave capable booster cells," in *Proc. IEEE Globecom Workshops (GC Wkshps)*, Dec. 2013, pp. 93–98.
[38] H. Peng, T. Yamamoto, and Y. Suegara, "LTE/WiGig RAN-level interworking architecture for 5G millimeter-wave heterogeneous networks," *IEICE Trans. Commun.*, vol. 98, no. 10, pp. 1957–1968, 2015.
[39] *S1 Application Protocol (S1AP)*, document TS 36.413 (v 12.4.0), 3GPP, Feb. 2015.
[40] S. Zhao, Z. Shao, H. Qian, and Y. Yang, "Online user-AP association with predictive scheduling in wireless caching networks," *Proc. IEEE Global Commun. Conf. (GLOBECOM)*, Singapore, Dec. 2017, pp. 1–7.
[41] O. Semiari, W. Saad, M. Bennis, and M. Debbah. (2017). "Performance analysis of integrated sub-6 GHz-millimeter wave wireless local area networks." [Online]. Available: https://arxiv.org/abs/1709.00988
[42] *Further advancements for E-UTRA Physical Layer Aspects*, document TR 36.814, 3GPP, Mar. 2010.
[43] X. Gao *et al.*, "Large-scale characteristics of 5.25 GHz based on wideband MIMO channel measurements," *IEEE Antennas Wireless Propag. Lett.*, vol. 6, pp. 263–266, Dec. 2007.
[44] T. S. Rappaport *et al.*, "Millimeter wave mobile communications for 5G cellular: It will work!" *IEEE Access*, vol. 1, pp. 335–349, May 2013.
[45] *D5.1 Channel Modeling and Characterization*, document FP7-ICT-608637, MiWEBA Project Deliverable, Jun. 2014. [Online]. Available: http://www.miweba.eu/wp-content/uploads/2014/07/MiWEBA D5.1 v1.01.pdf
[46] E. M. Mohamed, K. Sakaguchi, and S. Sampei, "Experimental work on WiGig coverage area management and beamforming training using Wi-Fi fingerprint," in *Proc. IEEE Consum. Commun. Netw. Conf. (CCNC)*, Jan. 2017, pp. 772–777.
[47] R. E. Rezagah, H. Shimodaira, G. K. Tran, K. Sakaguchi, and S. Nanba, "Cell discovery in 5G HetNets using location-based cell selection," in *Proc. IEEE Standards Commun. Netw. (CSCN)*, Oct. 2015, pp. 137–142.
[48] A. Abdelreheem, E. M. Mohamed, and H. Esmaiel, "Location-based millimeter wave multi-level beamforming using compressive sensing," *IEEE Commun. Lett.*, vol. 22, no. 1, pp. 185–188, Jan. 2018.

AHMED S. MUBARAK (S'18) received the B.E. degree in electrical engineering from South Valley University, Egypt, in 2001, and the M.Sc. degree in computer science from Assiut University, Egypt, in 2013. He is currently pursuing the Ph.D. degree in communication engineering with the Faculty of Engineering, Aswan University. He has been a Teacher Assistant at Sohag University since 2014. His research interests include 5G networks, millimeter-wave transmissions, and multi-in multi-out systems.

HAMADA ESMAIEL (M'18) received the B.E. degree in electrical engineering and the M.Sc. degree in wireless communications from South Valley University, Egypt, in 2005 and 2010, respectively, and the Ph.D. degree in communication engineering from the University of Tasmania, Australia, in 2015. In 2011, he joined the Wireless Communication Lab, Wonkwang University, Iksan, South Korea, as a Researcher Assistant. Since 2015, he has been an Assistant Professor with Aswan University, Egypt. His current research interests are 5G networks, Li-Fi technology, millimeter-wave transmissions, underwater communication, and multi-in multi-out systems. He is a Technical Committee Member in many international conferences and a reviewer in many international conferences, journals, and transactions. He is a General Co-Chair of the IEEE ISWC 2018.

EHAB MAHMOUD MOHAMED (M'10) received the B.E. degree in electrical engineering and the M.E. degree in computer science from South Valley University, Egypt, in 2001 and 2006, respectively, and the Ph.D. degree in information science and electrical engineering from Kyushu University, Japan, in 2012. From 2013 to 2016, he was a specially appointed Researcher with Osaka University, Japan. Since 2017, he has been an Associate Professor with Aswan University, Egypt. Since 2018, he has been an Associate Professor with Prince Sattam bin Abdulaziz University, Saudi Arabi. His current research interests are 5G networks, cognitive radio networks, millimeter-wave transmissions, Li-Fi technology, multi-in multi-out systems, and underwater communication. He is a Technical Committee Member in many international conferences and a reviewer in many international conferences, journals, and transactions. He is the General Chair of IEEE ITEMS 2016 and IEEE ISWC 2018.